High-Pressure Melting Curve of Zintl Sodium Silicide Na4Si4 by In Situ Electrical Measurements

Alexandre Courac, Yann Le Godec, Carlos Renero-Lecuna, Hicham Moutaabbid, Ram Kumar, Cristina Coelho-Diogo, Christel Gervais, David Portehault

High Pressure Melting Curve of Zintl Sodium Silicide Na_4Si_4 by *In Situ* Electrical Measurements

Alexandre Courac,[*,a] *Yann Le Godec,*[a] *Carlos Renero-Lecuna,*[a] *Hicham Moutaabbid,*[a] *Ram Kumar,*[b] *Cristina Coelho-Diogo,*[c] *Christel Gervais,*[b] *and David Portehault*[b]

[a] Sorbonne Université, CNRS, Muséum National d'Histoire Naturelle, IRD, Institut de Minéralogie, de Physique des Matériaux et de Cosmochimie (IMPMC), 75005 Paris, France

[b] Sorbonne Université, CNRS, Collège de France, Laboratoire de Chimie de la Matière Condensée de Paris (CMCP), 4 place Jussieu, F-75005, Paris, France

[c] Sorbonne Université, CNRS, Institut des Matériaux de Paris Centre, 4 place Jussieu, F-75005, Paris, France

AUTHOR INFORMATION

Corresponding Author

***** Corresponding author: alexandre.courac@upmc.fr

ABSTRACT. The inorganic chemistry of the Na-Si system at high pressure is fascinating, with a large number of interesting compounds accessible in the industrial pressure scale, below 10 GPa. Especially, Na_4Si_4 is stable in this whole pressure range, and thus plays an important role for understanding the thermodynamics and kinetics underlying materials synthesis at high pressures and high temperatures. In the present work, the melting curve of the Zintl compound Na_4Si_4 made of Na^+ and Si_4^{4-} tetrahedral cluster ions is studied at high pressures up to 5 GPa, by using *in situ* electrical measurements. During melting, the insulating Na_4Si_4 solid transforms into an ionic conductive liquid that can be probed through the conductance of the whole high-pressure cell, i.e. the system constituted of the sample, the heater and the high-pressure assembly. Na_4Si_4 melts congruently in the studied pressure range and its melting point increases with pressure with a positive slope dT_m/dp of 20(4) K/GPa.

KEYWORDS Sodium silicide, High pressure, Phase diagram, Melting curve

INTRODUCTION

The Zintl solid sodium silicide Na_4Si_4 bears Si species with negative oxidation state and built on $[Si_4]^{4-}$ tetrahedral clusters, which are surrounded by Na^+ cations on each face.[1-2] The presence of both covalent and ionic bonds in the structure imparts interesting chemical and physical attributes.[3] Na_4Si_4 itself may be considered as a strategic energy material in hydrogen technologies to generate hydrogen as a fuel (portable hydrogen fuel cell cartridges) and for high energy density storage of hydrogen under low pressure.[4] Besides, Na_4Si_4 is a promising precursor for the synthesis of extended Si frameworks and allotropes of technological relevance.[5-13] Na_xSi_{46} ($x \leq 8$) and Na_xSi_{136} ($x \leq 24$) (type-I and type-II clathrates, respectively) consisting of Si cages encapsulating Na have been reported from Na_4Si_4 decomposition.[14-17] Empty Si_{46} and Si_{136} frameworks also provide tunable band gap for thermoelectrics and photovoltaics with Si_{136} exhibiting a quasi-direct bandgap of ~2 eV.[15, 18] Recently Na_4Si_4 has been used as precursor to design a new high-pressure synthetic route to the narrow-bandgap silicon allotrope Si-III.[13, 19] As a starting material, Na_4Si_4 is a compound of choice, as compared to ductile metallic sodium, for high pressure synthesis, since it can be finely powdered, which is crucial for homogeneity of the product. In addition, it participates in the phase equilibria[11] and impacts crystallization kinetics[20] in the binary Na-Si system that holds great promise to discover new technologically relevant semiconducting Si allotropes and compounds in the high pressure range. This is exemplified by the high pressure clathrate $NaSi_6$[20-21] that leads by Na substraction to the new orthorhombic allotrope Si_{24} with quasi-direct bandgap of ~1.35 eV,[6] making this solid highly relevant for energy conversion.[22] Overall, Na_4Si_4 appears as an important starting or intermediate compound that participates in the Na-Si phase equilibria during high-pressure syntheses. However, our understanding of the high pressure-temperature phase diagram and more broadly of thermodynamic data of Na_4Si_4 is incomplete and relies sometimes on controversial reports.[23-25]

Na_4Si_4 at ambient pressure has two low- and high- temperature polymorphs, α- and β- respectively.[23,26] The temperature of the α-to-β transformation is ~885 K at ambient pressure.[24] An isosymmetric transformation of the monoclinic α form has been also reported above 10 GPa and 300 K, yielding γ-Na_4Si_4.[27] The equation-of-state for α-Na_4Si_4 below 10 GPa[27,28] suggests a bulk modulus B_0 = 24(1) GPa (B'_0 = 4). According to the density of the different polymorphs, β- and γ-Na_4Si_4 should exhibit lower and higher bulk modulus, respectively, but still close to that of the α form.[29-32]

In order to effectively use Na_4Si_4 as precursor for high-pressure syntheses, a detailed understanding of its high pressure-temperature phase diagram and physical behavior in the liquid state is an important requisite. With this objective, we have especially focused on the melting curve of Na_4Si_4. Because of their refractory behavior and high reactivity, assessing melting of compounds like Na_4Si_4 under HPHT conditions is a significant methodological challenge. Indeed, *in situ* X-ray diffraction (XRD) peaks are widened under HP and Na-Si solids and liquids react with most available thermocouples, thus hindering a precise evaluation of the melting temperature by regular XRD techniques. To overcome this limitation, we propose a new methodology to probe phase transitions, based on electrical conductivity measurements.

EXPERIMENTAL METHODS

Synthesis

The silicon (~325 mesh, 99%) and NaH (95%) powder swere obtained from Sigma-Aldrich. All the synthesis and manipulations were performed inside a glove-box and on a Schlenk line under Ar atmosphere. Na_4Si_4 was synthesized using a procedure adapted from the one

reported by Ma *et al.*[33] In a typical synthesis Si and NaH powders were mixed in 1:2.1 mole ratio and ball milled for 2 min at 20 Hz (Retsch MM400 ball mill airtight vials of 50 mL, one steel ball of 62.3 g and a diameter of 23 mm). The obtained homogeneous mixture was transferred to an h-BN crucible, covered with a lid and subsequently transferred inside a quartz tube. The reaction was performed at 420 °C for 90 hours under Ar. The product was obtained as a brown-black pellet with white residue on top. The white residue corresponded to NaOH and was carefully removed from the top of the pellet. The latter was crushed to obtain Na_4Si_4 powder.

Characterization

X-ray diffraction (XRD) was performed on a Bruker D8 Advance diffractometer operating at the Cu Kα wavelength, with a sample holder equipped with a plastic dome to maintain the sample under inert argon atmosphere. The crystallographic reference was obtained from the reference ICSD card 193513. The resulting grey powder (according to XRD, a = 12.17(2) Å, b = 6.55(1) Å, c = 11.15(2) Å, β = 119.0(3)°, space group No 15, C12/c1, which corresponds to the α-Na_4Si_4 polymorph)[26] was transferred and stored under argon. ^{29}Si and ^{23}Na magic angle spinning nuclear magnetic resonance (MAS NMR) experiments were performed on a 700 MHz AVANCE III Bruker spectrometer operating at 139.05 MHz using a 3.2 mm Bruker probe spinning at 20 kHz and at 185.20 MHz using a 4 mm Bruker probe spinning at 14 kHz respectively. A single-pulse excitation was used with a recycle delay of 500 s and 512 scans for ^{29}Si and of 1s and 24 scans for ^{23}Na. ^{29}Si and ^{23}Na chemical shifts were referenced to TMS and 0.1M NaCl (aq) respectively. The spectra were simulated with the DMFIT program.[34]

Electrical measurements at HPHT

High pressure experiments have been performed using an hydraulic "Paris-Edinburgh" (PE) press applying force on tungsten carbide opposite anvils that compress a high-pressure cell (Fig. 1a). High temperatures were achieved by resistive heating (graphite ceramic or plastified graphite material, Grafoil). The pressure was calibrated with the diamond Si equation-of-state by *in situ* XRD at the PSICHE beamline of synchrotron SOLEIL.[11] The temperature was calibrated with a Si melting standard at high pressure.[35] Graphite (as ceramic or in grafoil) is a material of choice to serve simultaneously as heater and capsule material, while being chemically inert versus the Na_4Si_4 melt at the temperatures of interest. A typical HP cell is shown in Fig. 1a, along with the corresponding equivalent circuit (Fig. 1c) used for electrical measurements, including the heater and the sample (in parallel connection to the middle part of the heater). An alternating current was used for heating the cell by the Joule effect, simultaneously, the total resistance of the heating chain (together with voltage, current and power) has been probed. Figure 1b shows the theoretically expected power-resistance curves in the case of metallic and graphite heaters for insulator-to-metal transformations.

The HPHT experiments of simultaneous *in situ* XRD and electrical measurements has been performed at ID06 beamline at ESRF using large-volume multianvil press.[36] Ceramic graphite has been used as a heating material, with non linear heating (Fig. 1d). Figures 1d and 1e show the validity of the methodology, i.e. the correlation of the resistance drop with changes in powder diffraction patterns using *R-t*, *P-t* and XRD vs time diagrams. However, constant (preferably linear power change) heating rate has to be used for reliable analysis to exclude artefacts non-related to sample electrical properties (e.g. green arrow on Fig. 1d and e). Ceramic graphite is also then the best materials. In the following experiments, we have favored the use of grafoil, which allows obtaining smooth *R-P* curves.

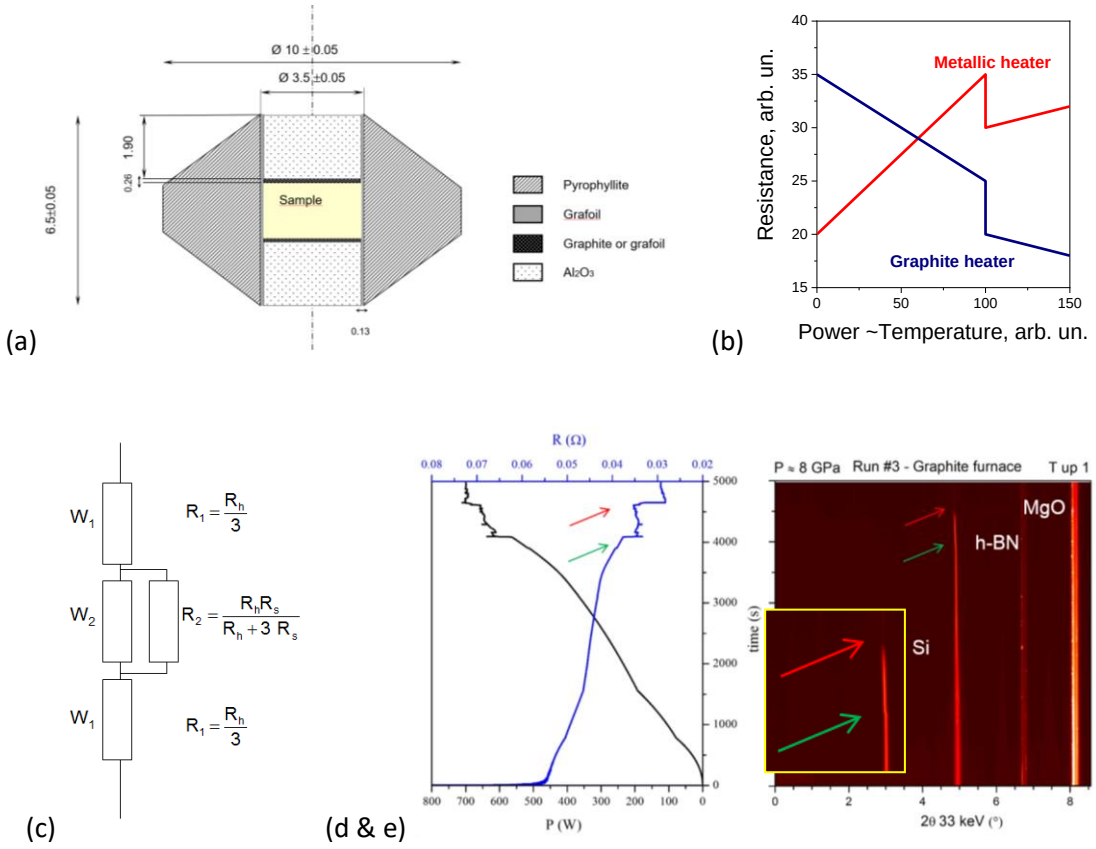

Figure 1. (a) High-pressure PE cell 10/3.5 for the electrical measurements of the (sample + heater) system. **(b)** Theoretical resistance curves of (sample + heater). The sample is an insulator below the critical power of 100 arb. un. and conducting, metallic above. **(c)** Electrical equivalent circuit of the (sample + heater) system with total resistance $2R_1+R_2$ (R_h – total heater resistance, R_s – sample resistance). **(d & e)** Simultaneous electrical (R and P vs t) and in situ XRD measurements of Si in the ceramic graphite heater, as an example of the methodology. The vertical axes in **d** and **e** represent time with (non-linear) heating above silicon melting temperature (**d**). Arrows indicate the simultaneous changes in resistance and XRD patterns. Inset in **e** is a zoom-in showing changes in the *d*-spacing of Si reflection: the red arrows correspond to melting. The green arrows are most probably due to a slight pressure drop.

RESULTS

The Na_4Si_4 compound studied in the present work was synthesized by reaction between sodium hydride and silicon. The XRD pattern (Fig. 2a) measured under inert atmosphere shows that Na_4Si_4 is the main phase, with trace amounts of Na and NaOH. TEM (Fig. 2b,c) shows that the particles are micron-size. The ^{29}Si MAS solid state NMR spectrum of Na_4Si_4 (Fig. 3a) shows signals at 361 and 365 ppm in excellent agreement with previously reported data[37] and corresponding to the two crystallographically different Si sites in the crystal structure (monoclinic, *C*2/*c*).[3] The upfield shift compared to pure silicon or silicon oxides is attributed to the electron donation from the electropositive Na to the electronegative Si.[38] Similarly, the ^{23}Na spectrum (Fig. 3b) shows two quadrupolar resonance patterns in nearly equal proportions and with isotropic chemical shift values of 56.5 ppm (Cq = 1.27 MHz, η = 0.8) and 49.7 ppm (Cq = 2.34 MHz, η = 0.25), corresponding to two crystallographically different Na sites in the crystal structure. The quadrupolar parameters of the two sites are significantly different, suggesting differences for the two sites in terms of electronic and symmetry environments. An additional signal on the ^{23}Na NMR spectrum, at ca. 20 ppm, corresponds to impurities and accounts for approximately 5% of the total amount of Na. It can be possibly assigned to NaOH.[39]

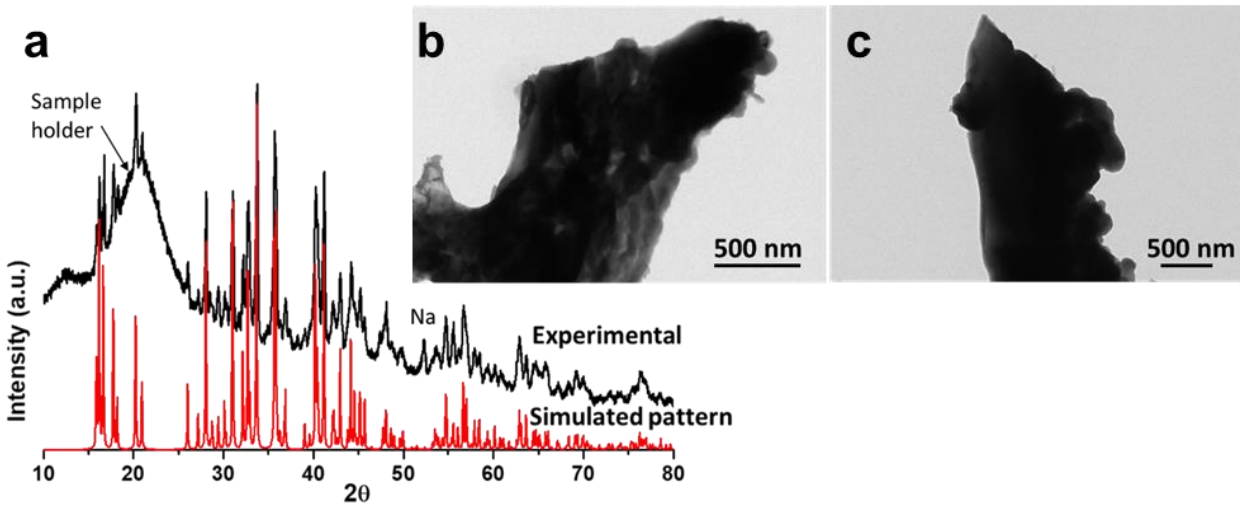

Figure 2. (a) Powder XRD pattern (black) of as-obtained Na_4Si_4. The calculated reference pattern for Na_4Si_4 is shown in red. A peak at ~52° corresponds to metallic sodium impurities. **(b, c)** TEM images of as-synthesized Na_4Si_4.

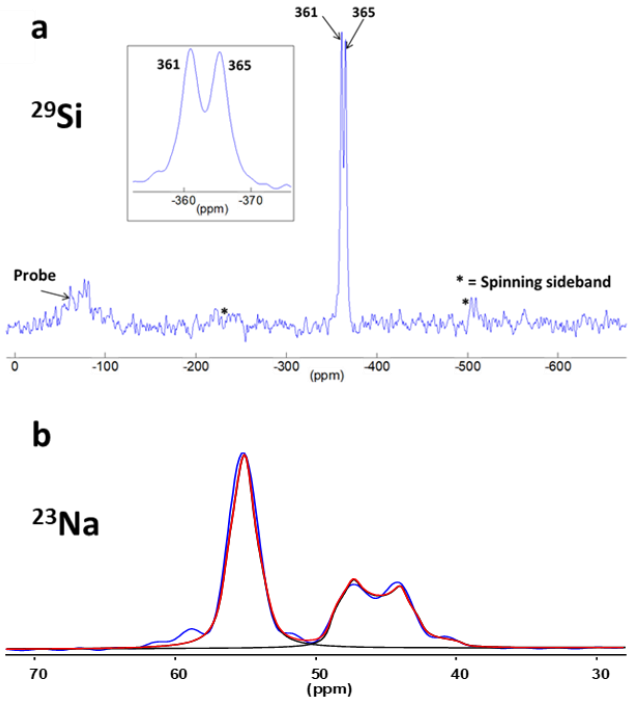

Figure 3. (a) ^{29}Si and (b) ^{23}Na solid-state NMR spectra of as-obtained Na_4Si_4.

Figure 4a shows typical power-resistance (*P-R*) curves for Si and Na_4Si_4. In the case of Si the *P-R* dependence prior to melting follows a quasi-linear decrease, typical for plastified grafoil.

Here we should note that in the case of ceramic graphite, the dependence is never so smooth, most probably because of the cracking of ceramics under pressure and, thus, of the modification of electrical contacts. Metallic heaters-capsules behave similar to grafoil, but with a quasi-linear increase of resistance. The Si *P*-*R* curve allows distinguishing three points related to melting: (1) onset, (2) inflection and (3) accomplishing melting powers. Each specific power cannot be attributed to a single temperature due to the temperature gradients inside the HP cell. Each of the three characteristic points on melting curve can be used for temperature calibration, thus resulting in three calibration curves (Fig. 4b). We favor the use of the inflection point as the best estimate, while onset and accomplishing points allow estimating the error bar. Actually, the three calibration curves just represent three different places in the cell: the hottest, intermediate and coldest places.

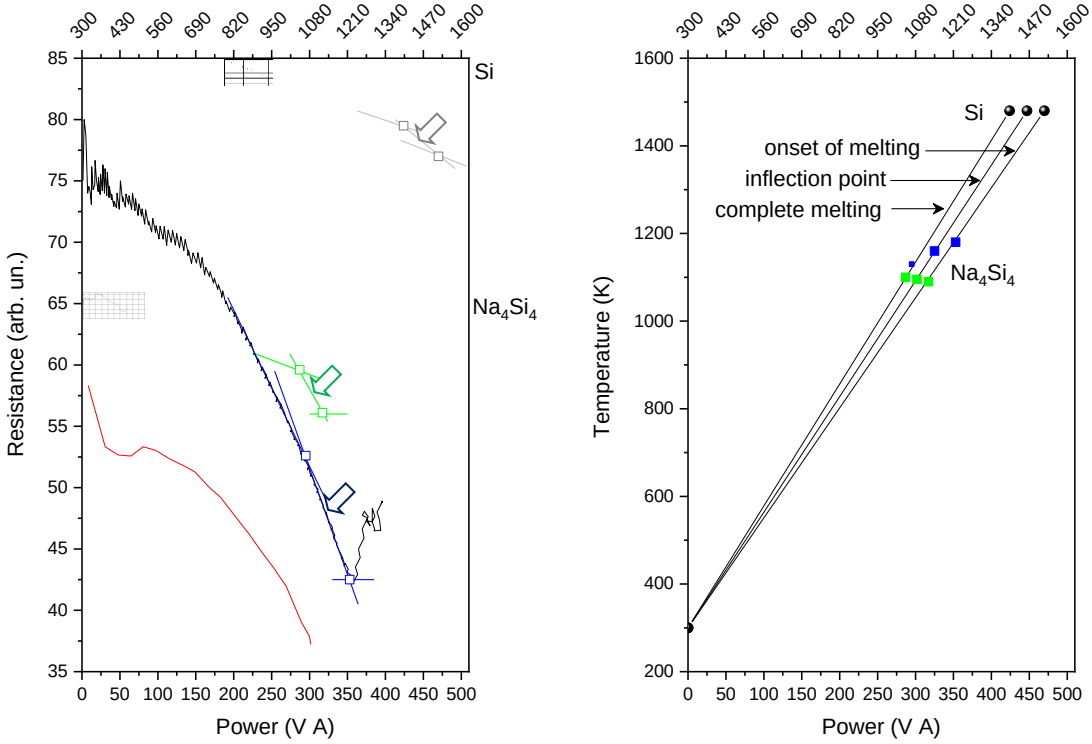

(a) (b)

Figure 4. (a) Experimental resistance curves of the (Na_4Si_4 + heater) system at 2, 4 and 5 GPa (green, red and blue eye-guide lines, respectively). The Si sample has been used as a temperature standard (melting at 1480 K at 4 GPa). The non-linear resistance behavior in (Na_4Si_4 + grafoil) system as compared to (Si + grafoil) can be explained by smaller hardness of Na_4Si_4 (and, therefore, higher deformation of the heater) and increase of the solid-state ionic conductivity when approaching melting. Arrows of corresponding color show the points attributed to the melting. The squiggles appear at the end of some curves because the power-resistance points are connected at increasing time, while the resistance may change at constant power during heating. **(b)** Silicon calibration curve (from the position of inflection point, $T = 300 + 2.64 \times P$) and temperature estimation of the Na_4Si_4 melting point at different pressures from onset, inflection and completion points on the resistance curves (2 and 5 GPa by green and blue squares, respectively).

The electrical behavior of Na_4Si_4 under heating is different from the ideal case of Si (Fig. 4a). The typical feature of melting can be clearly distinguished (green and blue lines allow distinguishing clearly the onset, inflection and completion points) by a change in the slope of resistance = f(power) curves. Similar to silicon, Na_4Si_4 is an insulator in the solid state (covalent Si and ionic Na_4Si_4 solids) and conductor in the liquid state (metallic Si and Na_4Si_4 ionic liquids). Visual analysis of recovered samples indicates that a transient drop of the resistance with subsequent increase in the resistance-power curve is characteristic of melting (black Na_4Si_4 curves at Fig. 4a, black circles at Fig. 5a). On the contrary, a strong resistance drop without subsequent resistance increase (red Na_4Si_4 curve at Fig. 4a, grey circle at Fig. 5a) cannot definitively indicate the melting (no melting features in recovered sample). The mechanism of such behavior is not clear so far, but no interaction between sodium silicide and graphite was observed at the temperatures studied. No correlation with a possible α-to-β

transformation could be evidenced either. All in all, the melting curve of Na_4Si_4 could be extracted (Fig. 5a) from the 2 and 5 GPa resistance curves (Fig. 4a). Theoretically, ionic conductivity can be evaluated from such experiments.[40] For such estimation the knowledge of sample size and shape during melting is crucial. However, in our case the powder was used as starting material, making it impossible to evaluate the sample dimensions under compression. Combined synchrotron X-ray imaging and electrical measurements on a sintered Na_4Si_4 sample could resolve this problem, but outstands the scope of the present work. One also needs to comment on the possible impact of contaminations (e.g. Na, NaOH mentioned above) on the melting temperature. The melt, once formed, enters into contact with the heater and/or escapes the central part of the HP cell with highest pressure. However, the quantity of Na and NaOH impurities and of related possible eutectic liquids corresponding to a maximum of about 5 mol. % of the total amount of Na, as evaluated from NMR. These amounts are so small that only the melting of the sample whole volume can cause noticeable resistance change (typically ~20-30% change observed herein). Possible chemical reactions with graphite may have occurred, but to a minor extent, as the heaters were always recovered after the experiments as being deformed, with no visible reaction on their walls. Such contaminations melting(s) and side reactions with the heater container may be responsible for the significant noise observed on the resistance curve at the initial heating stage (e.g. below 150 VA, Fig. 4a), which occurs in the domain of melting temperatures of these impurities. However, they cannot be account for the significant resistance drop observed at higher temperature, which we attribute to Na_4Si_4 melting.

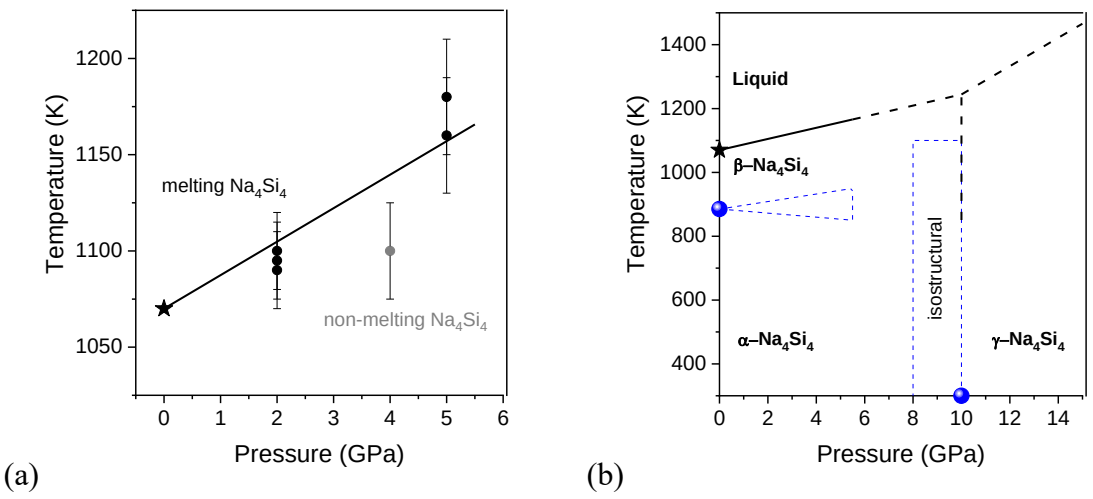

Figure 5. (a) Experimental melting curve of Na_4Si_4. The $T_m - p$ dependence is quasilinear (solid line) and follows the equation $T_m(K) = 1070 + 17.4 \times p(GPa)$ (the best estimate for linear dependence of melting curve has been obtained by weighted least square fit.). **(b)** High-pressure, high-temperature data on the phase diagram of Na_4Si_4. Solid symbols show the experimental data available from 24, 27. The solid line indicates the results of the present work. Blue dashed lines (guides for eye) delimit possible domains of localization of α/β and α/γ (observed experimentally)[27] equilibrium lines. Black dashed lines show extrapolated equilibria α/liquid and α/γ together with tentative γ/liquid line.

DISCUSSION

The positive slope of the melting curve of Na_4Si_4 is dT_m/dp = +17(2) K GPa^{-1}, which is indicative of positive melting volume change of $\Delta V_m = \Delta H_m \times (dT_m/dp) / T_m$. Using the estimation of ΔH_m ~204 kJ/mol,[23, 41] one can evaluate ΔV_m ~ 3.3 cm^3 mol^{-1} (or atomic volume change of 0.41 cm^3 mol^{-1}). It is interesting to note that Si itself shows negative dT_m/dp = -60 K GPa^{-1},[35] and ΔV_m = -1.8 cm^3 mol^{-1} according to thermochemical data (ΔH_m = 50.2 kJ mol^{-1})[41], while direct experimental measurements give ΔV_m = -(1.4-1.9) cm^3/mol.[42-43] Such a

negative dependence is typical for diamond-type crystal structures.[44-45] Sodium shows dT_m/dp = 87 K/GPa,[46] which combines with ΔH_m = 2.6 kJ mol^{-1} to give ΔV_m = +0.61 cm^3 mol^{-1}, close to experimentally observed +0.6 cm^3 mol^{-1}.[47]

Fig. 6 shows a non-linear dependence of the melting volume on the composition. Such a non-trivial dependence is related to the diversity of chemical species present in the solids and liquid. Na_4Si_4 liquid encompasses $[Si_4]^{4-}$ polyhedral clusters that do not allow significant volume decrease, in contrast with pure Si with significant difference in packings between solid diamond and atomic liquid structures. Also, if one follows the guide-for-the-eye curve (Fig. 6), the melting volume change for clathrate compounds in the Na-Si system are expected to be close to zero, which is to be confirmed (or refuted) experimentally. Theoretical simulations of open-framework Si clathrates suggest their strongly negative melting slopes[48-49] due to a dense liquid phase similar to ambient pressure Si liquid, thus rendering the clathrates (open frameworks + intercalated atoms) also strongly negative ΔV_m –even probably more than Si – if Si in Na-Si liquids has local structure similar to Si rather than clathrate-related structure(s).

Table 1. Thermodynamic data on melting of Na, Na_4Si_4 and Si. Bold values represent the experimental data from this work, non-bold values show the data from previous works (values given in italic – obtained by *ab initio* calculations).

Phase	dT_m/dp, K/GPa	ΔH_m, kJ mol^{-1}	$\Delta V_m^{calculated}$, cm^3 mol^{-1}	$\Delta V_m^{experimental}$, cm^3 mol^{-1}	T_m, K at 0.1 MPa
Na	87(7)	2.6	+0.61(5)	+0.6	371
Na_4Si_4	**+17(2)**	8×*25.5*	+8×**0.41**	--	1070
Si	-60(7)	50.2	-1.8(2)	-1.4 to -1.9	1687

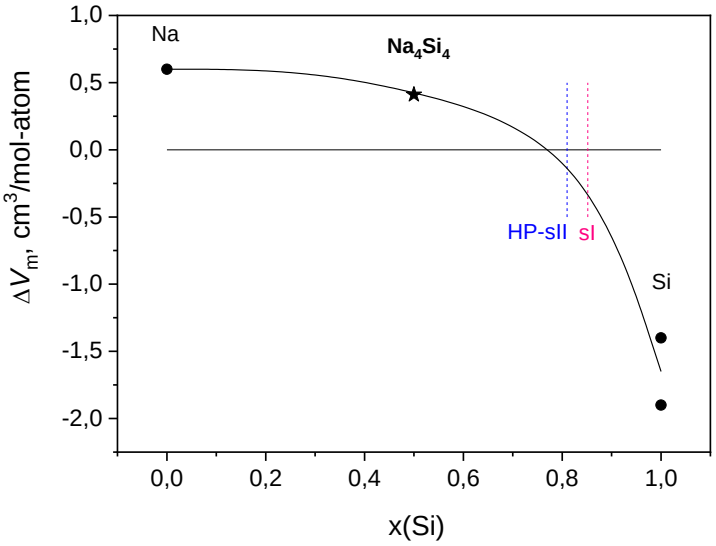

Figure 6. Melting volume ΔV_m (per mole of atoms, at melting temperature) of Na_4Si_4, in comparison with experimental values for Na[47] and Si.[42-43] The continuous thick black curve is a guide for the eye. The thin solid horizontal line corresponds to $\Delta V = 0$; while the blue and red dashed vertical lines show the composition of $Na_{30.5}Si_{136}$ (HP-sII) and Na_8Si_{46} (sI) clathrates respectively.

The established melting curve is shown as a black solid line on the tentative phase diagram of Na_4Si_4 at HPHT conditions (Fig. 5b). Linear extrapolation of the melting curve to high pressures and its intersection with the 10 GPa isobar (corresponding to the room-temperature isosymmetric (isostructural) α-to-γ transformation, which should be of first order (or discontinuous) with $\Delta V \neq 0$)[50], allows giving the first estimate for a triple point of Na_4Si_4 at ~10 GPa and ~1250 K. For high-pressure synthesis, the importance of this triple point for syntheses at ~10 GPa may be very high. Additional *in situ* studies are then required to probe the phase diagram of Na_4Si_4 at such high pressures. In order to get thermodynamically

consistent estimate for the melting curve of Na_4Si_4 above 10 GPa (melting of γ-phase), we have use the high-temperature approximation (previously used, for example, for the construction of high-temperature part of boron phase diagram[51]), suggesting constant ΔV, ΔH and ΔS for such couple of phases. The only lacking value $\Delta V_{\alpha/\gamma}$ = -8×0.32 $cm^3\ mol^{-1}$, that cannot be established as a combination of known values (using relationships $\Delta X_{x/y} = -\Delta X_{y/z}$ and $\Delta X_{x/y} = \Delta X_{x/z} + \Delta X_{z/y}$), has been established using experimental data.[27]

The above reported results also shed some light on the mechanism of synthesis of Na-Si clathrates at HPHT conditions, observed in previous *in situ* and *ex situ* experiments.[11] In fact, the formation of a high-pressure clathrate compound $Na_{30.5}Si_{136}$ of structural type II encapsulating two sodium atoms in the same silicon polyhedral cages[52] (as compared to one atom in the case of stoichiometric $Na_{24}Si_{136}$ compound) has been observed at temperatures ~300 K below the melting point of Na_4Si_4 (i.e. at ~800 K).[11] The experimentally established eutectic melting temperature (equilibrium Na_4Si_4+Si↔liquid) is just ~50 K lower than that for pure Na_4Si_4,[24] which is indicative of the solid state interaction between Si and Na_4Si_4 at temperatures below melt formation.

As a Zintl compound, Na_4Si_4 is built from Na^+ cations and $[Si_4]^{4-}$ clusters isostructural to the P_4 molecule constituting white phosphorus (α wP). Hence, Na_4Si_4 is an ionic solid, while α wP is a molecular solid. Interestingly, the differences in properties of Na_4Si_4 derived from our study and those reported for α wP are consistent with the differences in cohesion. As expected, the ionic cohesion of Na_4Si_4 provides it with much lower point melting point at 1080 K than the molecular solid α wP at 317 K.[53-54] Likewise, our work indicates that the ionic solid Na_4Si_4 has a melting slope of 20 K/GPa, ten times lower than the molecular solid α wP.[53-54] Previous high pressure studies have also shown that the bulk modulus of α wP is ~6.7(5) GPa,[53] while the presence of Na^+ ions distributed between the negatively charged

silicon tetrahedral leads to more than three times lower compressibility with bulk modulus of 24 GPa.

CONCLUSIONS

Finally, the melting curve of Na_4Si_4 has been established using the methodology of total resistance measurements (graphite or grafoil heater and sample in parallel electrical connection scheme). This method allows overpassing the problems of high reactivity (with electrodes or environment) and low crystal symmetry with polymorphism (for reliable XRD observation). Our results have shown the positive slope of Na_4Si_4 melting curve, while the estimated value of the melting volume is close to that of sodium. Our results allow predicting a triple point of the liquid/α/γ phases at ~ 10 GPa and 1250 K, i.e. potentially in the domain of interest for the synthesis of high-pressure intermetallic clathrates and silicon allotropes.

ACKNOWLEDGMENT

We thank Mss. Silvia Pandolfi for assistance in high-pressure experiments. The work of A.C. was financially supported by Institut Universitaire de France (IUF). C.R.L. and D.P. thanks LabEx MATISSE program AAP 2016 - POST-DOCTORANTS. D.P. and R.K. thank the CNRS for funding. The French Région Ile de France - SESAME program is acknowledged for financial support (700 MHz NMR spectrometer). The *in situ* XRD experiments were performed on beamline ID06-LVP at the European Synchrotron Radiation Facility (proposal CH-5431). We are grateful to Drs. W. Crichton and K. Spector at the ESRF for providing assistance in using beamline ID06-LVP.

REFERENCES

1. Nesper, R., Bonding Patterns in Intermetallic Compounds. *Angewandte Chemie International Edition in English* **1991,** *30* (7), 789-817.
2. Fässler, T. F., *Zintl Ions: Principles and Recent Developments* Springer Berlin Heidelberg, 2011.
3. Goebel, T.; Prots, Y.; Haarmann, F., Refinement of the crystal structure of tetrasodium tetrasilicide, Na4Si4. *Zeitschrift für Kristallographie - New Crystal Structures* **2008,** *223* (3), 187.
4. Agrawal, T.; Ajitkumar, R.; Prakash, R.; Nandan, G., Sodium Silicide As A Hydrogen Source For Portable Energy Devices: A Review. *Materials Today: Proceedings* **2018,** *5* (2, Part 1), 3563-3570.
5. Iversen, B. B.; Palmqvist, A. E. C.; Cox, D. E.; Nolas, G. S.; Stucky, G. D.; Blake, N. P.; Metiu, H., Why are Clathrates Good Candidates for Thermoelectric Materials? *Journal of Solid State Chemistry* **2000,** *149* (2), 455-458.
6. Kim, D. Y.; Stefanoski, S.; Kurakevych, O. O.; Strobel, T. A., Synthesis of an open-framework allotrope of silicon. *Nat. Mater.* **2015,** *14* (2), 169-173.
7. Kume, T.; Ohashi, F.; Nonomura, S., Group IV clathrates for photovoltaic applications. *Japanese Journal of Applied Physics* **2017,** *56* (5S1), 05DA05.
8. Connetable, D.; Timoshevskii, V.; Masenelli, B.; Beille, J.; Marcus, J.; Barbara, B.; Saitta, A. M.; Rignanese, G. M.; Melinon, P.; Yamanaka, S.; Blase, X., Superconductivity in Doped sp^3 Semiconductors: The Case of the Clathrates. *Phys. Rev. Lett.* **2003,** *91* (24), 247001.
9. Wang, Q.; Xu, B.; Sun, J.; Liu, H.; Zhao, Z.; Yu, D.; Fan, C.; He, J., Direct Band Gap Silicon Allotropes. *J. Amer. Chem. Soc.* **2014,** *136* (28), 9826-9829.
10. Kurakevych, O. O.; Le Godec, Y.; Crichton, W. A.; Strobel, T. A., Silicon allotropy and chemistry at extreme conditions. *Energy Procedia* **2016,** *92*, 839-844.
11. Jouini, Z.; Kurakevych, O. O.; Moutaabbid, H.; Le Godec, Y.; Mezouar, M.; Guignot, N., Phase boundary between Na-Si clathrates of structures I and II at high pressures and high temperatures. *J. Superhard Mater.* **2016,** *38* (1), 66-70.
12. Kurakevych, O. O.; Le Godec, Y.; Crichton, W. A.; Guignard, J.; Strobel, T. A.; Zhang, H. D.; Liu, H. Y.; Diogo, C. C.; Polian, A.; Menguy, N.; Juhl, S. J.; Alem, N.; Gervais, C., Synthesis of Bulk BC8 Silicon Allotrope by Direct Transformation and Reduced-Pressure Chemical Pathways (v6ol 55, pg 8943, 2016). *Inorg. Chem.* **2016,** *55* (19), 9949-9949.
13. Kurakevych, O. O.; Le Godec, Y.; Crichton, W. A.; Guignard, J.; Strobel, T. A.; Zhang, H. D.; Liu, H. Y.; Diogo, C. C.; Polian, A.; Menguy, N.; Juhl, S. J.; Gervais, C., Synthesis of Bulk BC8 Silicon Allotrope by Direct Transformation and Reduced-Pressure Chemical Pathways. *Inorg. Chem.* **2016,** *55* (17), 8943-8950.
14. Kasper, J. S.; Hagenmul, P.; Pouchard, M.; Cros, C., Clathrate Structure of Silicon and Na_xSi_{136} (x=11). *Science* **1965,** *150* (3704), 1713-1714.
15. Himeno, R.; Kume, T.; Ohashi, F.; Ban, T.; Nonomura, S., Optical absorption properties of Na_xSi_{136} clathrate studied by diffuse reflection spectroscopy. *Journal of Alloys and Compounds* **2013,** *574*, 398-401.
16. Simon, P.; Tang, Z.; Carrillo-Cabrera, W.; Chiong, K.; Böhme, B.; Baitinger, M.; Lichte, H.; Grin, Y.; Guloy, A. M., Synthesis and Electron Holography Studies of Single Crystalline Nanostructures of Clathrate-II Phases KxGe136 and NaxSi136. *Journal of the American Chemical Society* **2011,** *133* (19), 7596-7601.
17. Ramachandran, G. K.; Dong, J.; Diefenbacher, J.; Gryko, J.; Marzke, R. F.; Sankey, O. F.; McMillan, P. F., Synthesis and X-Ray Characterization of Silicon Clathrates. *Journal of Solid State Chemistry* **1999,** *145* (2), 716-730.

18. Gryko, J.; McMillan, P. F.; Marzke, R. F.; Ramachandran, G. K.; Patton, D.; Deb, S. K.; Sankey, O. F., Low-density framework form of crystalline silicon with a wide optical band gap. *Physical Review B* **2000,** *62* (12), R7707-R7710.
19. Zhang, H. D.; Liu, H. Y.; Wei, K. Y.; Kurakevych, O. O.; Le Godec, Y.; Liu, Z. X.; Martin, J.; Guerrette, M.; Nolas, G. S.; Strobel, T. A., BC8 Silicon (Si-III) is a Narrow-Gap Semiconductor. *Phys. Rev. Lett.* **2017,** *118* (14), 6.
20. Guerette, M.; Ward, M. D.; Lokshin, K. A.; Wong, A. T.; Zhang, H. D.; Stefanoski, S.; Kurakevych, O.; Le Godec, Y.; Juhl, S. J.; Alem, N.; Fei, Y. W.; Strobel, T. A., Synthesis and Properties of Single-Crystalline Na_4Si_{24}. *Cryst. Growth Des.* **2018,** *18* (12), 7410-7418.
21. Kurakevych, O. O.; Strobel, T. A.; Kim, D. Y.; Muramatsu, T.; Struzhkin, V. V., Na-Si Clathrates Are High-Pressure Phases: A Melt-Based Route to Control Stoichiometry and Properties. *Cryst. Growth Des.* **2013,** *13* (1), 303-307.
22. Linghu, J.; Shen, L.; Yang, M.; Xu, S.; Feng, Y. P., Si_{24}: An Efficient Solar Cell Material. *The Journal of Physical Chemistry C* **2017,** *121* (29), 15574-15579.
23. Hao, D.; Bu, M.; Wang, Y.; Tang, Y.; Gao, Q.; Wang, M.; Hu, B.; Du, Y., THERMODYNAMIC MODELING OF THE Na–X (X = Si, Ag, Cu, Cr) SYSTEMS. *J. Min. Metall. Sect. B 48* **2012,** *48* (2), 273 - 282.
24. Morito, H.; Yamada, T.; Ikeda, T.; Yamane, H., Na–Si binary phase diagram and solution growth of silicon crystals. *Journal of Alloys and Compounds* **2009,** *480* (2), 723-726.
25. Mali, A.; Petric, A., EMF Measurements of the Na-Si System. *Journal of Phase Equilibria and Diffusion* **2013,** *34* (6), 453-458.
26. Hohmann, E., Silicides and Germanides of the Alkali Metals. *Z. Anorg. Chem.* **1948,** *257* (1–3), 113–126.
27. Cabrera, R. Q.; Salamat, A.; Barkalov, O. I.; Leynaud, O.; Hutchins, P.; Daisenberger, D.; Machon, D.; Sella, A.; Lewis, D. W.; McMillan, P. F., Pressure-induced structural transformations of the Zintl phase sodium silicide. *Journal of Solid State Chemistry* **2009,** *182* (9), 2535-2542.
28. Murnaghan, F. D., The compressibility of media under extreme pressures. *Proct. Natl. Acad. Sci.* **1944,** *30*, 244.
29. Le Godec, Y.; Kurakevych, O. O.; Munsch, P.; Garbarino, G.; Solozhenko, V. L., Equation of state of orthorhombic boron, gamma-B-28. *Solid State Commun.* **2009,** *149* (33-34), 1356-1358.
30. Mukhanov, V. A.; Kurakevych, O. O.; Solozhenko, V. L., The interrelation between hardness and compressibility of substances and their structure and thermodynamic properties. *J. Superhard Mater.* **2008,** *30* (6), 368-378.
31. Solozhenko, V. L.; Kurakevych, O. O.; Le Godec, Y.; Brazhkin, V. V., Thermodynamically Consistent p-T Phase Diagram of Boron Oxide B_2O_3 by in Situ Probing and Thermodynamic Analysis. *J. Phys. Chem. C* **2015,** *119* (35), 20600-20605.
32. Kurakevych, O. O.; Solozhenko, V. L., 300-K equation of state of rhombohedral boron subnitride, B13N2. *Solid State Commun.* **2009,** *149* (47-48), 2169-2171.
33. Ma, X.; Xu, F.; Atkins, T. M.; Goforth, A. M.; Neiner, D.; Navrotsky, A.; Kauzlarich, S. M., A versatile low temperature synthetic route to Zintl phase precursors: Na_4Si_4, Na_4Ge_4 and K_4Ge_4 as examples. *Dalton Trans.* **2009,** (46), 10250-10255.
34. Massiot, D.; Fayon, F.; Capron, M.; King, I.; Le Calvé, S.; Alonso, B.; Durand, J.-O.; Bujoli, B.; Gan, Z.; Hoatson, G., Modelling one- and two-dimensional solid-state NMR spectra. *Magnetic Resonance in Chemistry* **2002,** *40* (1), 70-76.
35. Kubo, A.; Wang, Y.; Runge, C. E.; Uchida, T.; Kiefer, B.; Nishiyama, N.; Duffy, T. S., Melting curve of silicon to 15 GPa determined by two-dimensional angle-dispersive diffraction using a Kawai-type apparatus with X-ray transparent sintered diamond anvils. *J. Phys. Chem. Solids* **2008,** *69* (9), 2255-2260.

36. Guignard, J.; Crichton, W. A., The large volume press facility at ID06 beamline of the European synchrotron radiation facility as a High Pressure-High Temperature deformation apparatus. *Rev. Sci. Instrum.* **2015,** *86* (8), 085112.
37. Mayeri, D.; Phillips, B. L.; Augustine, M. P.; Kauzlarich, S. M., NMR Study of the Synthesis of Alkyl-Terminated Silicon Nanoparticles from the Reaction of SiCl4 with the Zintl Salt, NaSi. *Chemistry of Materials* **2001,** *13* (3), 765-770.
38. Tegze, M.; Hafner, J., Electronic structure of semiconducting alkali-metal silicides and germanides. *Physical Review B* **1989,** *40* (14), 9841-9845.
39. Wang, J.; Sen, S.; Yu, P.; Browning, N. D.; Kauzlarich, S. M., Synthesis and spectroscopic characterization of P-doped Na4Si4. *Journal of Solid State Chemistry* **2010,** *183* (11), 2522-2527.
40. Mukhanov, V. A.; Solozhenko, V. L., On electrical conductivity of melts of boron and its compounds under pressure. *J. Superhard Mater.* **2015,** *37* (4), 289-291.
41. Dinsdale, A. T., SGTE data for pure elements. *Calphad* **1991,** *15* (4), 317-425.
42. Glazov, V. M.; Shchelikov, O. D., Volume changes during melting and heating of silicon and germanium melts. *High Temperature* **2000,** *38* (3), 405-412.
43. Rhim, W. K.; Chung, S. K.; Rulison, A. J.; Spjut, R. E., Measurements of thermophysical properties of molten silicon by a high-temperature electrostatic levitator. *International Journal of Thermophysics* **1997,** *18* (2), 459-469.
44. Sokolov, P. S.; Mukhanov, V. A.; Chauveau, T.; Solozhenko, V. L., On melting of silicon carbide under pressure. *J. Superhard Mater.* **2012,** *34* (5), 339-341.
45. Hall, H. T., The Melting Point of Germanium as a Function of Pressure to 180,000 Atmospheres. *The Journal of Physical Chemistry* **1955,** *59* (11), 1144-1146.
46. Luedemann, H. D.; Kennedy, G. C., Melting curves of lithium, sodium, potassium, and rubidium to 80 kilobars. *Journal of Geophysical Research* **1968,** *73* (8), 2795-2805.
47. Makarenko, I. N.; Nikolaenko, A. M.; Ivanov, V. A.; Stishov, S. M., Equation of state of alkali metals: Sodium. *JETP* **1975,** *42* (5), 875-879.
48. Wilson, M.; McMillan, P. F., Crystal-Liquid Phase Relations in Silicon at Negative Pressure. *Phys. Rev. Lett.* **2003,** *90* (13), 135703.
49. Daisenberger, D.; McMillan, P. F.; Wilson, M., Crystal-liquid interfaces and phase relations in stable and metastable silicon at positive and negative pressure. *Physical Review B* **2010,** *82* (21), 214101.
50. Christy, A., Isosymmetric structural phase transitions: phenomenology and examples. *Acta Crystallographica Section B* **1995,** *51* (5), 753-757.
51. Solozhenko, V. L.; Kurakevych, O. O., Equilibrium p-T Phase Diagram of Boron: Experimental Study and Thermodynamic Analysis. *Scientific Reports* **2013,** *3*.
52. Yamanaka, S.; Komatsu, M.; Tanaka, M.; Sawa, H.; Inumaru, K., High-Pressure Synthesis and Structural Characterization of the Type II Clathrate Compound $Na_{30.5}Si_{136}$ Encapsulating Two Sodium Atoms in the Same Silicon Polyhedral Cages. *J. Amer. Chem. Soc.* **2014,** *136* (21), 7717-7725.
53. Clark, S. M.; Zaug, J. M., Compressibility of cubic white, orthorhombic black, rhombohedral black, and simple cubic black phosphorus. *Physical Review B* **2010,** *82* (13), 134111.
54. Bridgman, P. W., TWO NEW MODIFICATIONS OF PHOSPHORUS. *Journal of the American Chemical Society* **1914,** *36* (7), 1344-1363.

TOC GRAPHICS

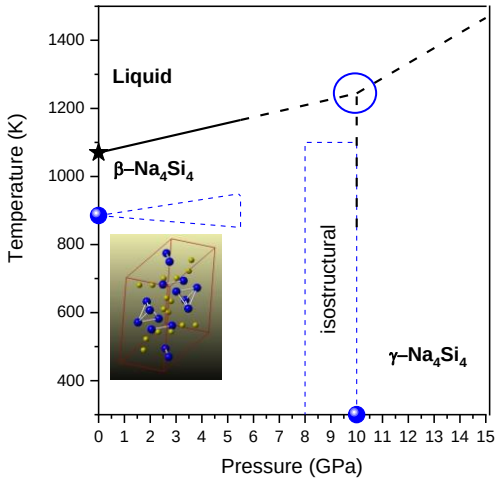

The inorganic chemistry of the Na-Si system at high pressure is fascinating, with a large number of interesting compounds accessible in the industrial pressure scale, below 10 GPa. Na_4Si_4, a main stable compound in this pressure range and that which is participating in all high-pressure synthetic routes of clathrate silicon frameworks, melts congruently and its melting point increases with pressure with a positive slope.